Clays and Clay Minerals, Vol. 50, No. 6, 710–725, 2002.

ZEOLITIZATION OF A PHONOLITIC ASH FLOW BY GROUNDWATER IN THE LAACH VOLCANIC AREA, EIFEL, GERMANY

FRANZ BERNHARD* AND ULRIKE BARTH-WIRSCHING

Institut für Technische Geologie und Angewandte Mineralogie, Technische Universität Graz, Rechbauerstraße 12, A-8010 Graz, Austria

Abstract—Field and experimental studies were performed to understand the formation conditions of the Nettetal zeolite deposit, Laach volcanic area, Germany. This deposit shows pronounced small- (cm) and large-scale (tens of meters) variations of zeolitization, despite the same phonolitic precursor glass throughout the occurrence. Zeolitization of the pyroclastic ash flow is restricted to three distinct layers that are 0.15 to 10 m thick and separated by fresh ash. The glassy matrix is altered to chabazite, phillipsite, analcime and K-feldspar in various combinations, whereas the pumice clasts are altered predominantly to chabazite. Mass changes during zeolite formation appear to be small, and Ca enrichment in chabazite and phillipsite may have occurred after their formation by cation exchange.

The zeolites and zeolite assemblages observed in the Nettetal deposit were experimentally reproduced by reacting the phonolitic glass at 100−200ºC with distilled water and 0.01 M alkaline solutions as well as with varying solid/liquid ratios and grain-sizes. Chabazite and phillipsite represented metastable transition phases with respect to analcime and K-feldspar. A high solid/liquid ratio accelerated the conversion of glass to zeolites.

None of the classic models of zeolite formation is fully applicable to the Nettetal deposit. The most probable environment for zeolitization in this deposit is the stagnant fringe water zone immediately above the groundwater table. In this zone, representing a relatively closed system, favorable solution compositions for zeolite formation could have been developed rather quickly by glass-water interaction, which is not possible within the more thoroughly flushed deeper parts of the groundwater system. The three distinct zeolite layers are probably the result of temporarily changing groundwater levels.

Key Words—Ash Flow, Eifel, Experimental Zeolitization, Fringe Water Zone, Groundwater, Laach Volcanic Area, Phonolitic Glass, Zeolites.

INTRODUCTION

Economically important zeolite deposits are commonly formed by the alteration of vitric volcanic materials in sedimentary environments (Hay, 1977). Two major types of hydrologic systems in these environments have been distinguished: (1) closed systems of saline, alkaline lakes; and (2) open, groundwater systems. The Yellow Neapolitan Tuff was regarded by Hay and Sheppard (1977) as an example of the second type. The trachytic glass of these ~12,000 year old deposits was altered chiefly to phillipsite, chabazite and small amounts of analcime. Recently, contrasting genetic models have been proposed for this deposit. De'Gennaro *et al.* (2000) related zeolitization to conservation of magmatic heat and phreatomagmatic water within the ash flows, effectively resulting in zeolite formation in a closed system. Hall (1998), however, rejected such a possibility, because typically acid volcanic waters do not favor zeolite formation. He suggested zeolitization by a flushing of the volcaniclastic sediments with fresh water, followed by subsequent reheating.

* E-mail address of corresponding author:
bernhard@egam.tu-graz.ac.at

The Nettetal zeolite deposit in the Laach volcanic area, Eifel, Germany, is of similar age and composition to the Neapolitan Yellow Tuff and is characterized by zeolitized layers intercalated with fresh phonolitic ashes. Previous studies established the presence of chabazite, phillipsite and analcime as newly formed minerals from glass shards and pumice clasts (Frechen, 1971; Höller and Wirsching, 1974; Adabbo *et al.*, 1994). The distribution of these zeolites differs (1) between layers, (2) within a given layer, and (3) between matrix and pumice clasts. Höller and Wirsching (1974) showed that all three zeolites can form by the reaction of phonolitic glass with pure water, depending on temperature and reaction time. Nevertheless, many questions are still to be answered concerning the distribution of these zeolites within or between different zeolitized layers, the different zeolitization of pumice clasts and matrix, and the formation of Ca-rich chabazite from Na-rich, phonolitic vitric material. Both a field and an experimental study, investigating the alteration of the phonolitic glass in a closed system with low-concentrated alkaline solutions at temperatures between 100 and 200ºC during reaction times up to 400 days as well as in a slightly open system, have been conducted to answer these questions and to gain insight into the formation processes of this relatively young zeolite deposit in a low-alkalinity setting.

GEOLOGY

The ~12,900 year old Laacher See volcanic eruption produced at least 5 km^3 of mainly phonolitic material formed by pyroclastic and phreatomagmatic processes (Bogaard and Schmincke, 1984, 1995). Three stages of eruption can be distinguished in the proximal deposits: the first stage (Lower Laacher See Tephra) consists mainly of fallout pumice deposits; the second stage (Middle Laacher See Tephra) is characterized by abundant pyroclastic flows and subordinate fallout deposits; and the third, phreatomagmatic stage (Upper Laacher See Tephra) comprises surge breccias, dunes and flows (Harms and Schmincke, 2000). The magma chamber was chemically zoned, resulting in highly differentiated phonolitic compositions at the base and more mafic phonolite at the top of the volcaniclastic succession (Harms and Schmincke, 2000).

Pyroclastic flows of the second stage were predominantly deposited in valleys northeast (Brohltal) and southeast (Nettetal) of the volcanic vent (Figure 1). The partly zeolitized Nettetal ash flow is ~5 km southeast of the volcanic vent; it extends subparallel to the Nettetal and is as thick as 35 m. The ash is very poorly sorted and consists of fine-grained phonolitic glass shards and clasts of phonolitic pumice ($\leqslant$10 cm in size), basalt, fragments of Devonian schists, pebbles and grains of quartz, and pyrogenic minerals, such as sanidine, clinopyroxene, hornblende, phlogopite, haüyne, magnetite and titanite. Twenty six of thirty ash samples studied by Jandausch (1980) had a median grain-size <2 mm. Fallout pumice deposits of the same eruptive stage overlay and underlay the flow deposit. Jandausch (1980) recognized 14 individual flow units, deposited within a few days or even a few hours. Frechen (1971), however, distinguished only three flows.

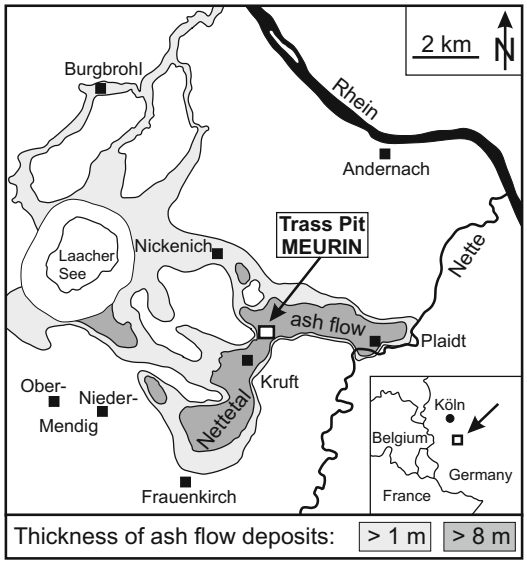

Figure 1. Distribution of pyroclastic ash flow deposits of the Laacher See volcanic eruption (after Bogaard and Schmincke, 1984, modified).

MATERIALS AND METHODS

Fresh and zeolitized samples were collected along a nearly vertical section in the northwestern part of the Trass Pit Meurin (Figure 1), in which the Nettetal ash flow is best exposed. Some samples were also collected in the eastern part of the pit. Zeolitized samples were broken with a hammer into 1–2 cm large pieces and crushed gently with a pestle to 1–5 mm large fragments. Pumice clasts and matrix fragments were then separated by hand picking and ground.

Analytical techniques

X-ray powder diffraction (XRD) analyses of natural samples and experimental products were performed with a Philips PW1840 diffractometer using CuKα radiation. Sample powders were front loaded in aluminum holders and compacted with a glass plate. Semiquantitative analyses were done by comparison of the XRD patterns with those of reference materials, natural and synthetic zeolites, using as many peaks as possible for quantification. The precision of sample preparation and measurement was ~2% (one standard deviation).

Polished thin-sections of natural samples and grain mounts of experimental products were examined by scanning electron microscopy and energy-dispersive X-ray analysis (SEM-EDX), using a SEM JEOL JSM-6310, equipped with an Oxford Link Isis EDX spectrometer, operated at 15 kV accelerating voltage and ~2 nA probe current. Natural minerals (albite, adularia, garnet, titanite, tephroite) were used as standards, and the focused electron beam was scanned over such a large area that Na-loss was negligible (5×5 to 10×10 µm). Due to surface roughness, measurements of grain mounts were prone to larger analytical errors than analyses of polished section, especially concerning K/Na ratios.

Bulk-sample chemical composition was measured by X-ray fluorescence (XRF) on fused glass discs with a Philips PW1404 wavelength-dispersive X-ray spectrometer. Twenty one international geochemical reference samples were used for calibration, and precision and accuracy were monitored by repeated measurement of USGS reference materials GSP-2 (granodiorite), G-2 (granite) and W-2 (diabase) (Govindaraju, 1994). All average values are reported as median to account for the small number of analyses of individual minerals (mostly <10) and to minimize the effect of outliers on the average (Lister, 1982; Rock *et al.*, 1987).

Experimental synthesis procedures

Experimental starting materials of different grain-sizes were prepared from zeolite-free overlying fallout pumice deposits by stepwise grinding and dry sieving.

https://doi.org/10.1346/000986002762090245 Published online by Cambridge University Press

The composition of experimental starting materials was very close to that of the fresh glasses of the Trass Pit Meurin (Tables 1 and 2).

Experiments were performed in unstirred 70 mL Teflon-coated stainless steel vessels, heated in drying cabinets. Temperature was controlled to ±5ºC. After programmed reaction time, vessels were allowed to cool to room temperature and solids were separated from solutions by paper filters and washed at least three times with distilled water or until a pH of ~7 was reached.

The experiments on the formation of zeolites in a closed system can be divided into two major groups. The first group investigated the influence of solution chemistry, temperature, and reaction time within a given solid/liquid ratio and grain-size. Samples of 0.5 g of ground pumice (<63 μm) were reacted with 25 mL of 0.01 M NaOH, 0.005 M NaOH + 0.005 M NaCl, 0.005 M NaOH + 0.005 M KOH, or distilled water at 100, 150 and 200ºC for 8−400 days. The possibility of the direct formation of Ca,K-rich chabazite was investigated in experiments using a 0.005 M $Ca(OH)_2$ solution at 200ºC. The second group of experiments explored the influence of different grain-sizes and solid/liquid ratios at otherwise constant conditions. Samples of 0.5, 1.0 and 2.0 g of pumice having a grain-size of <63 μm, samples of 2.0 g of pumice having a grain-size of 0.2−1.0 mm, and individual pumice fragments weighing ~2 g were reacted with 25 mL of distilled water at 200ºC for 8−80 days. Experiments simulating zeolitization in a slightly open system were also performed at 200ºC with distilled water by replacing the solution in the reaction vessel after 8 days of reaction with fresh distilled water.

These experimental alteration conditions were chosen to be as close as possible to natural ones. Temperatures used ($\geqslant$100ºC), however, were probably higher than in nature in order to accelerate glass dissolution as well as zeolite formation. Nevertheless, the experimental synthesis results can be used to discuss the influence of the factors mentioned above on the formation of chabazite, phillipsite, analcime, and K-feldspar in the Nettetal zeolite deposit.

Cation-exchange experiments on Na,K-rich chabazite produced in the experiments were performed with water containing 90 mg/L Ca, 16 mg/L Mg, 8 mg/L Na (groundwater of Graz) in batch mode; 0.1 g Na,K-rich chabazite was reacted with 1 L of water at 20ºC. Water was replaced weekly for 5 weeks.

Table 1. Median of SEM-EDX analyses (wt.%) of glasses in the Trass Pit Meurin and of experimental starting material <63 μm. For comparison, bulk chemical data for sample EX <63 μm by XRF are given in Table 2.

Sample	Fresh pumice interior	Glass relics interior	Glass shards surface	EX <63 μm surface
n	14	7	6	6
SiO_2	59.10	59.46	59.49	60.06
TiO_2	0.19	0.20	0.21	0.24
Al_2O_3	21.42	21.45	22.55	21.80
Fe_2O_3	1.96	1.99	2.11	1.81
MnO	0.36	0.20	0.24	0.29
MgO	0.15	0.18	0.22	0.11
CaO	0.84	0.88	0.70	0.87
Na_2O	9.94	9.66	8.47	9.07
K_2O	6.04	5.98	6.01	5.75
Si/Al molar	2.34	2.35	2.25	2.34

Analyses normalized to 100 wt.% on a volatile-free basis
EX: starting material for experiments; *n*: number of analyses

FIELD RESULTS

Field relations and mineralogy

The most conspicuous feature of the Nettetal zeolite deposit is the occurrence of three distinct zeolitized layers throughout the pit area of ~0.2 km^2, characterized by a significantly increased induration compared with that of the friable fresh ash. These subhorizontal layers are, from top to bottom, 0.15−0.2 m, 2 m and 12 m thick (Figure 2, layers A, B, C, respectively). The contact between zeolitized layers and non-zeolitized, fresh ash is sharp within 1−2 cm. Layer A and C are continuous, but layer B represents individual zeolitized lenses of 5−20 m length and ~2 m thickness. Zeolitized layers locally crosscut boundaries between flow units (Jandausch, 1980). Zeolitization of pumice clasts, recognizable by a color change from white to yellow or gray-green, decreases towards the contact with fresh ash over a distance of 0.5−2 m in layer C. Layer B contains zeolitized pumice clasts in the lower part, and layer A contains predominantly fresh pumice clasts. In contrast to the ash matrix, pumice clasts become more friable with increasing zeolitization.

The material of layer B has been used as a pozzolanic additive since Roman times; layer C is currently being exploited for the same purpose ("Rheinischer Traß") and layer B material is used for building stones.

Authigenic minerals are chabazite, phillipsite, analcime and K-feldspar. These minerals appear to have grown at the expense of glass and possibly quartz (Figure 3b); all other components of the ash are unaltered. The distribution of zeolites and K-feldspar in the glassy matrix is very different from that in the pumice clasts, and therefore glassy matrix and pumice clasts must be considered separately.

The pumice clasts in layers B and C are invariably altered to predominantly chabazite (>80 wt.%), with small amounts of phillipsite and analcime. Age relationships between the three zeolites are not entirely clear, but the first zeolite formed was chabazite, as can be judged from growth of phacolitic chabazite on glass surfaces into open vesicles in the upper parts of layers B and C (Figure 3a). Chabazite phacolites in totally altered pumice clasts have a diameter of 30−50 μm.

https://doi.org/10.1346/000986002762090245 Published online by Cambridge University Press

Table 2. XRF analyses (wt.%) of experimental starting materials and of fresh and zeolitized pumice clasts of the Trass Pit Meurin. For sample locations see Figures 2 and 4. For comparison, surface chemical data for sample EX <63 μm by EDX are given in Table 1.

Sample	EX <63 μm	EX 0.2–1 mm	EX leach <63 μm	EX leach 0.2–1 mm	EX-P1	EX-P2	A2-P1 Fresh	FA3-P1 Fresh	FA3-P2 Fresh	FA3-P3 Fresh	FA4-P1 Fresh	FA4-P2 Fresh	B1-P2 Fresh	FA5-P1 Fresh	FA5-P2 Fresh
SiO_2	58.67	58.46	59.40	59.39	59.02	59.11	58.10	58.48	58.10	58.21	58.30	57.56	58.14	58.16	57.92
TiO_2	0.227	0.228	0.235	0.232	0.280	0.290	0.269	0.263	0.236	0.242	0.271	0.319	0.253	0.260	0.249
Al_2O_3	21.87	21.80	22.25	22.07	21.40	21.19	21.90	21.62	21.80	21.79	21.68	21.65	21.64	21.60	21.60
Fe_2O_3	2.150	2.103	2.231	2.164	2.246	2.167	2.341	2.233	2.066	2.083	2.240	2.369	2.146	2.144	2.095
MnO	0.313	0.321	0.328	0.326	0.261	0.243	0.276	0.267	0.277	0.275	0.281	0.288	0.276	0.278	0.277
MgO	0.106	0.113	0.135	0.118	0.149	0.174	0.238	0.169	0.118	0.122	0.156	0.238	0.135	0.152	0.132
CaO	0.986	0.951	1.029	1.009	1.234	1.295	1.732	1.090	1.026	1.091	1.113	1.391	1.191	1.053	1.087
Na_2O	9.47	9.42	8.14	8.27	8.45	8.42	8.39	9.39	9.61	9.84	9.27	9.46	9.26	9.69	9.54
K_2O	6.053	6.020	6.111	6.022	6.356	6.441	6.197	6.033	6.125	6.035	6.186	5.957	6.304	6.117	6.267
P_2O_5	0.033	0.030	0.035	0.034	0.044	0.047	0.058	0.042	0.036	0.036	0.039	0.065	0.041	0.040	0.037
Total	99.878	99.437	99.896	99.635	99.440	99.377	99.501	99.587	99.394	99.724	99.536	99.297	99.386	99.494	99.204
LOI	3.22	3.22	5.94	5.90	3.34	2.67	4.96	2.57	2.76	2.62	3.41	3.35	3.54	2.66	2.77
Si/Al molar	2.28	2.28	2.27	2.28	2.34	2.37	2.25	2.30	2.26	2.27	2.28	2.26	2.28	2.28	2.28

Sample	FA7-P1 Fresh	FA7-P2 Fresh	FA7-P3 Fresh	FA7-P4 Fresh	FA7-P5 Fresh	B2-P2 Cbz	B3-P1 Cbz	B4-P1 Cbz	C2-P6 Cbz	C4-P3 Cbz	C6-P5 Cbz	C7-P3 Cbz
SiO_2	58.05	57.94	58.26	58.26	58.34	61.66	59.46	60.20	60.49	59.99	59.54	61.01
TiO_2	0.296	0.287	0.268	0.238	0.238	0.220	0.230	0.226	0.170	0.217	0.196	0.249
Al_2O_3	21.66	21.55	21.64	21.84	21.87	21.07	22.38	21.57	22.01	21.93	21.45	21.68
Fe_2O_3	2.282	2.410	2.258	2.065	2.139	2.004	2.112	2.073	1.976	2.110	2.002	2.313
MnO	0.285	0.279	0.268	0.276	0.272	0.189	0.279	0.261	0.232	0.293	0.245	0.267
MgO	0.143	0.213	0.197	0.114	0.129	0.918	0.552	0.909	0.956	1.125	0.186	1.377
CaO	1.114	1.168	1.132	1.071	1.028	6.544	7.515	6.034	5.773	3.288	1.076	2.925
Na_2O	9.68	9.26	9.64	9.82	9.78	1.28	1.39	1.93	1.98	3.87	6.87	3.90
K_2O	6.065	6.012	6.035	6.070	6.030	5.683	5.661	6.763	6.253	7.276	8.622	6.952
P_2O_5	0.039	0.046	0.039	0.033	0.032	0.052	0.047	0.049	0.045	0.045	0.022	0.043
Total	99.614	99.165	99.737	99.787	99.858	99.620	99.626	100.015	99.885	100.144	100.209	100.716
LOI	2.56	2.33	2.35	2.57	2.43	14.94	14.00	13.32	14.78	13.35	11.18	12.46
Si/Al molar	2.27	2.28	2.28	2.26	2.26	2.48	2.25	2.37	2.33	2.32	2.36	2.39

Analyses are given on a volatile-free basis
EX: starting materials for experiments; EX leach: 0.5 g treated with 25 mL distilled water at 200ºC for 8 days; EX-P1, EX-P2: pumice fragments, weighing ~2 g, used in experiments
FA: fresh pumice clasts within fresh ash; A, B, C: pumice clasts within zeolitized layers A, B, C, respectively; A2 *etc.* refer to locations given in Figures 2 and 4
Cbz: pumice clast replaced by chabazite; LOI: loss on ignition

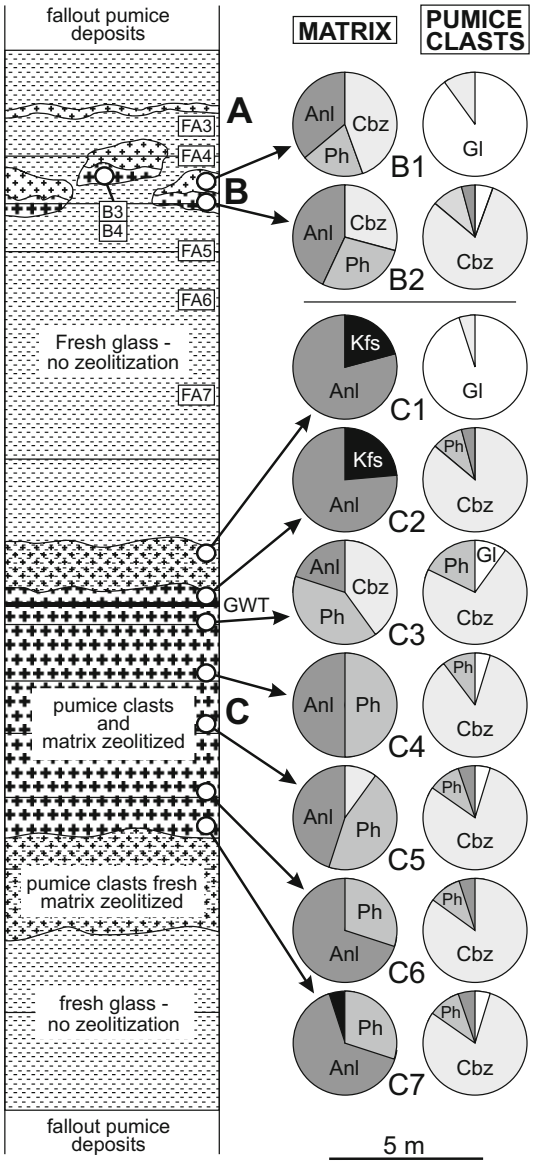

Figure 2. Simplified cross-section through the partly zeolitized ash flow of the Nettetal as exposed in the Trass Pit Meurin. Cross-section below groundwater table (GWT) is partly derived from core drillings (Jandausch, 1980). Locations of samples are indicated. Sample B4 was collected in the eastern part of the pit. Gl = glass, Cbz = chabazite, Ph = phillipsite, Anl = analcime, Kfs = K-feldspar.

The authigenic mineralogy of the matrix can vary within centimeters. Layer A was sampled in detail, and the uppermost portion consists predominantly of chabazite, whereas the remaining part is composed of chabazite, analcime and lesser amounts of phillipsite (Figure 4). The matrix of layer B consists of chabazite, phillipsite, and analcime (Figure 2). Layer C is the mineralogically most diverse, ranging from chabazite + phillipsite + analcime to analcime + K-feldspar (Figure 2). What appears to be newly-formed K-feldspar is particularly abundant in the uppermost part of layer C, just above the present groundwater table. Overgrowth features suggest that chabazite was the earliest and K-feldspar the latest authigenic phase formed (Figure 3a,b,d). K-feldspar overgrows pyrogenic sanidine and authigenic analcime as well, strongly suggesting an authigenic origin. The structural state of the authigenic K-feldspar appears to be high sanidine, (Goldsmith and Laves, 1954; Wright, 1968) but it could not be determined with confidence by XRD because of too many overlapping lines and admixture of pyrogenic sanidine. The grain-size of the zeolites ranges from 5 to 15 μm in all matrix samples, whereas the K-feldspar reaches only 3 μm.

Chemical characterization of pumice clasts and glass shards

The glass composition of pumice clasts and shards as well as fresh bulk pumice clasts and ash sieve fractions were analyzed to establish the range of chemical variation in various starting materials. The surfaces of fresh glass shards, glass of fresh pumice clasts and small glass relics within nearly totally zeolitized pumice clasts were analyzed using SEM-EDX (Table 1). The compositions were phonolitic, and Si/Al ranged from 2.25 to 2.35. Analyses of interior parts of glass shards gave slightly higher Na contents than analyses on the surface (Table 1). This might be due to the early stages of leaching of the glass surface, but it could also be an analytical artifact due to surface roughness. The glass chemistry is the same as that of the Middle Laacher See Tephra, subunit B (Harms and Schmincke, 2000).

Fresh, bulk-pumice clasts, 0.8−2.0 g in size, also showed narrow chemical variability. Variation within a sample was the same as variation between different samples and the median Si/Al of the 14 analyzed pumice clasts was 2.28 (Table 2, Figure 5). The <63 μm ash fraction also showed restricted chemical variability throughout the deposit, but TiO_2 and Fe_2O_3 were higher and Na_2O was lower than in pumice clasts (Table 3, Figure 5). Silica (and free quartz), TiO_2, Fe_2O_3, MgO and CaO increased, and Al_2O_3, Na_2O and K_2O decreased with grain-size of the sieve fraction, due to greater amounts of pyrogenic and epiclastic, non-glassy components in the coarser fractions.

Chemistry of zeolites and K-feldspar

The Si/Al ratios of the zeolites encountered ranged from 2.32 to 2.74 (Table 4). These values were close to or slightly higher than that of the glass (2.25−2.35). Within individual samples, the Si/Al of the chabazite was consistently slightly lower than that of phillipsite. The Si/Al ratios of analcime ranged from 2.45 to 2.59,

https://doi.org/10.1346/000986002762090245 Published online by Cambridge University Press

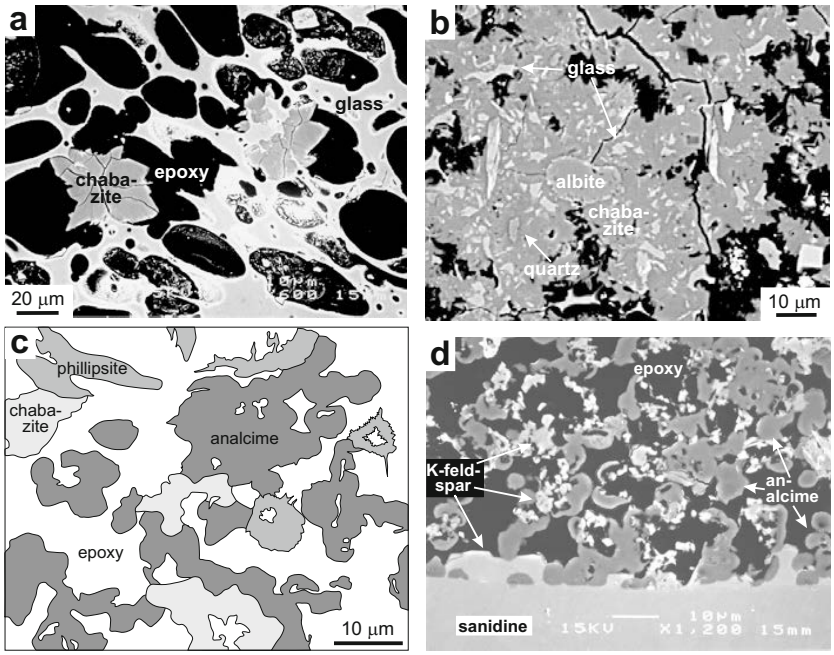

Figure 3. Back-scattered electron images of various stages of zeolite formation in the Nettetal zeolite deposit, Laach volcanic area, Germany. (a) Phacolitic chabazite on glass in vesicles of a pumice clast. Pumice clast of layer B, sample B1. (b) Massive chabazite with glass relics and possibly corroded quartz. Matrix of layer A, sample A1. (c) Intimate intergrowth of chabazite, phillipsite and analcime. Matrix of layer B, sample B2. (d) Analcime and K-feldspar. Newly formed K-feldspar overgrows analcime and pyrogenic sanidine as well. Matrix of layer C, sample C2.

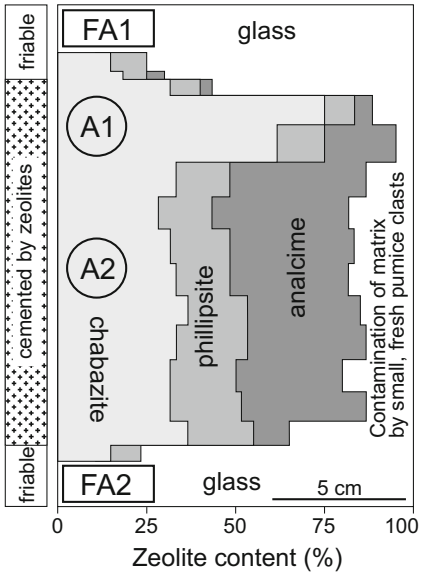

Figure 4. Distribution of zeolites within the matrix of the uppermost zeolitized layer (layer A), located at a depth of ~5 m below the land surface. Locations of samples are indicated.

and accompanying chabazite and phillipsite can have higher or lower Si/Al than the analcime. The Si/Al of a given zeolite did not seem to be a function of its mode of occurrence, *i.e.* in pumice clasts or in matrix.

The exchangeable cations content varied widely and generally differed from that of the glass. Chabazite crystals above the present groundwater table (layer A, B) were Ca,K-rich, but below the groundwater table, their composition ranged from Ca,K-rich to Na,K-rich (Table 4, Figure 6). Phillipsite showed the same compositional trends as chabazite, but it was usually less Ca-rich (Table 4, Figure 6). Analcime was near the Na end-member throughout the deposit (Table 4, Figure 6).

Authigenic K-feldspar was characterized by high Fe_2O_3 (median 1.74 wt.%) and K_2O contents, compared with pyrogenic sanidine found in the deposit (Table 4).

Bulk sample chemistry and mass changes

Bulk analyses of fresh and zeolitized pumice clasts showed the same compositional trends as SEM-EDX analyses of the fresh glass and individual zeolite crystals (Tables 2 and 4). An assessment of mass change is feasible for MgO, CaO, Na_2O and K_2O, using TiO_2 as an immobile monitor in an isocon plot (Figure 7; Grant, 1986). The composition of the fresh pumice is represented by the median of 13 bulk analyses. Most significant is the $\leqslant$10-fold enrichment of both CaO

https://doi.org/10.1346/000986002762090245 Published online by Cambridge University Press

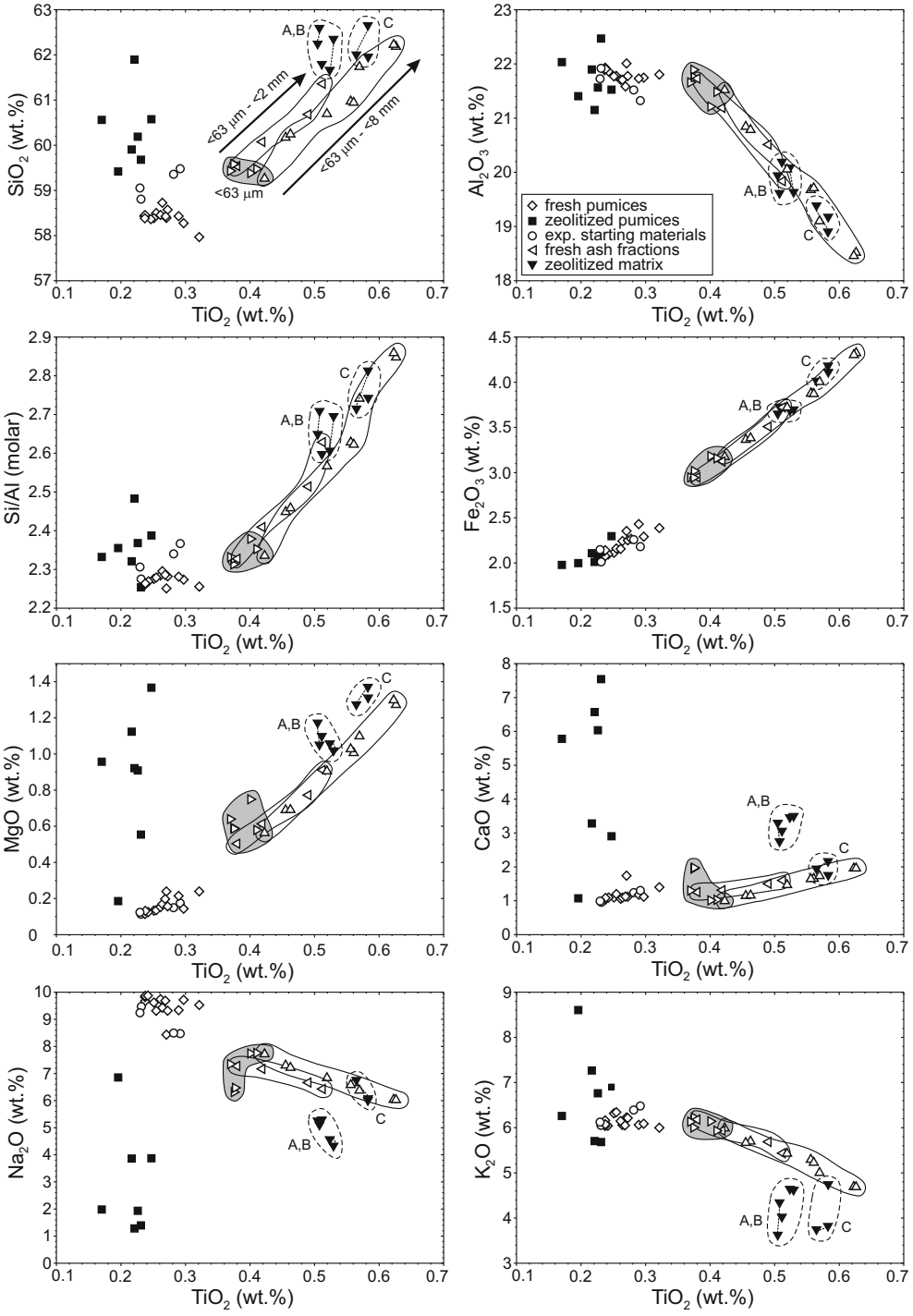

Figure 5. Chemical variation diagrams for experimental starting materials, fresh and zeolitized pumice clasts, fresh ash sieve fractions and zeolitized matrix samples of the Nettetal zeolite deposit. Shaded field outlines composition of ash fractions <63 µm. Arrows indicate compositional trends of increasing ash sieve size fractions for two samples. Broken lines connect matrix samples separated from the same specimen. A, B: matrix samples from layer A and B, respectively (chabazite + phillipsite + analcime); C: matrix samples from layer C (analcime + K-feldspar). Data normalized to 100 wt.% on a volatile-free basis.

https://doi.org/10.1346/000986002762090245 Published online by Cambridge University Press

Table 3. XRF analyses (wt.%) of fresh ash sieve fractions and zeolitized matrix samples of the Trass Pit Meurin. For sample locations see Figures 2 and 4.

Sample	FA1 <63 µm	FA2 <63 µm	FA3 <63 µm	FA3 <0.2 mm	FA3 <0.63 µm	FA3 <2 mm	FA4 <63 µm	FA5 <63 µm	FA6 <63 µm	FA7 <0.63 µm	FA7 <0.2 mm	FA7 rep <0.2 mm	FA7 <0.63 µm	FA7 <1 mm	FA7 <2 mm
SiO_2	59.52	59.55	59.51	60.08	60.51	61.19	59.67	59.86	59.14	58.92	60.04	59.89	60.56	60.65	60.56
TiO_2	0.376	0.377	0.378	0.417	0.487	0.509	0.373	0.406	0.410	0.420	0.461	0.453	0.518	0.553	0.557
Al_2O_3	21.86	21.73	21.72	21.18	20.44	19.77	21.73	21.37	21.35	21.40	20.72	20.75	20.01	19.57	19.59
Fe_2O_3	2.931	3.006	2.935	3.113	3.489	3.701	2.948	3.198	3.131	3.159	3.373	3.350	3.716	3.856	3.849
MnO	0.257	0.255	0.263	0.255	0.251	0.248	0.266	0.260	0.259	0.257	0.251	0.250	0.244	0.241	0.245
MgO	0.585	0.581	0.498	0.608	0.765	0.904	0.637	0.750	0.571	0.561	0.690	0.688	0.904	1.023	1.001
CaO	1.917	1.945	1.227	1.283	1.468	1.571	1.277	0.992	0.996	0.997	1.162	1.149	1.472	1.643	1.651
Na_2O	6.45	6.28	7.24	7.14	6.61	6.37	7.34	7.77	7.68	7.68	7.20	7.27	6.83	6.55	6.62
K_2O	5.976	6.202	6.157	5.915	5.651	5.400	6.136	6.170	5.879	5.958	5.683	5.644	5.421	5.271	5.198
P_2O_5	0.057	0.060	0.060	0.060	0.077	0.090	0.058	0.068	0.061	0.063	0.075	0.077	0.091	0.097	0.091
Total	99.929	99.986	99.988	100.051	99.748	99.753	100.435	100.844	99.477	99.415	99.655	99.521	99.766	99.454	99.362
LOI	6.06	5.40	4.24	3.84	3.63	3.40	4.54	3.31	3.04	2.99	2.83	2.78	2.61	2.52	2.55
Si/Al molar	2.31	2.33	2.32	2.41	2.51	3.65	2.33	2.38	2.35	2.34	2.46	2.45	2.570	2.63	2.62

Sample	FA7 <4 mm	FA7 <8 mm	FA7 rep <8 mm	A2-M1 zeolit.	B1-M1 zeolit.	B1-M2. zeolit.	B2-M1 zeolit.	B2-M2 zeolit.	C1-M1 zeolit.	C1-M2 zeolit.	C2-M2 zeolit.
SiO_2	61.57	61.88	62.08	61.77	62.26	62.27	62.08	61.47	62.58	61.69	62.27
TiO_2	0.568	0.623	0.621	0.511	0.505	0.505	0.527	0.522	0.582	0.562	0.586
Al_2O_3	19.05	18.43	18.42	20.18	19.51	19.95	19.55	20.02	18.88	19.29	19.27
Fe_2O_3	3.995	4.305	4.294	3.720	3.705	3.649	3.679	3.674	4.175	3.991	4.130
MnO	0.240	0.246	0.250	0.242	0.247	0.247	0.253	0.254	0.240	0.230	0.221
MgO	1.097	1.267	1.296	1.097	1.044	1.172	1.013	1.053	1.368	1.266	1.317
CaO	1.735	1.956	1.960	3.053	2.727	3.291	3.475	3.444	2.154	1.929	1.756
Na_2O	6.37	6.01	6.03	5.28	5.07	5.25	4.30	4.54	5.99	6.714	6.10
K_2O	4.994	4.671	4.685	4.019	4.316	3.622	4.596	4.622	3.811	3.723	4.763
P_2O_5	0.104	0.116	0.117	0.094	0.097	0.094	0.101	0.097	0.111	0.112	0.104
Total	99.723	99.504	99.753	99.966	99.481	100.050	99.574	99.710	99.891	99.503	100.517
LOI	2.50	2.44	2.42	7.74	7.64	8.92	8.15	8.65	6.01	5.58	6.11
Si/Al molar	2.74	2.85	2.86	2.60	2.71	2.65	2.69	2.61	2.81	2.71	2.74

Analyses are given on a volatile-free basis
FA: fresh ash
A, B, C: matrix of zeolitized layers A, B, C, respectively
FA1 *etc*. refer to locations given in Figures 2 and 4
rep: second glass disc prepared from the same sample powder
zeolit.: zeolitized
LOI: loss on ignition

Table 4. Median of SEM-EDX analyses (oxides in wt.%) of zeolites and K-feldspar in the Trass Pit Meurin. Formulae for chabazite, phillipsite, analcime and K-feldspar are calculated on 24, 32, 96 and 8 O atoms, respectively. For sample locations see Figures 2 and 4.

Sample	A1	A2	A2	A2	A2	B1	B1	B1	B1	B2	B2	B2	B2	B2
Location	Matrix	Pumice	Matrix	Matrix	Matrix	Pumice	Matrix	Matrix	Matrix	Pumice	Pumice	Matrix	Matrix	Matrix
Mineral	Cbz	Cbz	Cbz	Ph	Anl	Cbz	Cbz	Ph	Anl	Cbz	Ph	Ch	Ph	Anl
n	6	8	9	10	7	7	7	6	3	15	9	5	6	8
SiO_2	48.65	49.07	50.41	57.19	58.74	48.69	49.33	54.05	57.15	52.51	56.09	46.16	47.74	57.27
Al_2O_3	17.61	17.71	16.51	17.74	19.23	17.54	16.83	16.99	19.74	16.67	17.48	16.78	16.61	19.06
Fe_2O_3	0.39	0.19	0.57	0.68	1.10	0.32	0.51	0.71	0.75	0.57	0.78	0.67	0.51	0.54
MgO	0.18	0.38	0.79	–	–	0.64	0.69	–	–	1.47	–	0.26	–	–
CaO	6.50	5.75	5.20	3.92	0.27	6.49	5.15	3.11	0.28	4.61	2.78	5.48	4.13	0.10
Na_2O	0.40	0.28	0.27	0.75	10.31	0.44	0.43	1.44	11.09	0.38	1.75	0.63	0.73	10.42
K_2O	6.14	6.68	5.77	8.64	1.01	4.66	6.59	10.12	1.22	4.81	9.16	7.04	8.23	0.65
Total	79.87	80.06	79.52	88.92	90.66	78.78	79.53	86.42	90.23	81.02	88.04	77.02	77.95	88.04
Si	8.32	8.36	8.56	13.12	34.46	8.34	8.45	12.96	33.89	8.65	13.07	8.26	12.66	34.48
Al	3.55	3.55	3.30	4.80	13.30	3.54	3.40	4.80	13.80	3.24	4.80	3.54	5.19	13.52
Fe^{3+}	0.05	0.02	0.07	0.12	0.49	0.04	0.07	0.13	0.33	0.07	0.14	0.09	0.10	0.24
Mg	0.05	0.10	0.20	–	–	0.16	0.17	–	–	0.36	–	0.07	–	–
Ca	1.19	1.05	0.94	0.96	0.17	1.19	0.95	0.80	0.18	0.81	0.69	1.05	1.17	0.06
Na	0.13	0.09	0.09	0.33	11.73	0.14	0.14	0.67	12.75	0.12	0.79	0.22	0.38	12.16
K	1.34	1.45	1.25	2.53	0.76	1.0	21.44	3.10	0.92	1.01	2.72	1.61	2.78	0.50
E%	−8.80	−6.70	−7.00	2.60	7.50	−7.50	−9.10	−8.10	0.70	−5.00	0.70	−10.70	−3.90	7.60
Si/Al	2.34	2.35	2.59	2.74	2.59	2.36	2.49	2.70	2.46	2.67	2.72	2.33	2.44	2.55

Sample	C1	C1	C2	C2	C2	C2	C2	C3	C4	C5	C6	C6	C6	C6	C7	C7	C7	C7	C7	
Location	Matrix	Matrix	Pumice	Pumice	Pumice	Matrix	Matrix	Pumice	Pumice	Pumice	Pumice	Pumice	Matrix	Matrix	Pumice	Pumice	Matrix	Matrix	Matrix	
Mineral	Anl	Kfs	Cbz	Ph	Anl	Anl	Kfs	Cbz	Cbz	Cbz	Cbz	Ph	Ph	Anl	Cbz	Ph	Ph	Anl	Kfs	San
n	7	9	21	10	3	9	7	10	7	8	14	6	5	4	24	8	5	6	2	16
SiO_2	59.84	64.67	50.58	56.30	58.57	55.47	65.03	49.37	50.09	50.97	52.02	55.71	55.70	60.68	51.66	58.17	50.43	58.35	68.32	65.15
Al_2O_3	20.50	16.65	17.59	18.36	19.76	19.00	16.77	16.75	18.12	17.87	17.80	18.30	20.29	21.04	17.77	18.67	18.45	19.65	18.15	19.23
Fe_2O_3	0.44	1.77	0.22	0.35	0.36	0.61	1.91	0.34	0.45	0.45	0.57	0.61	0.53	0.70	0.42	0.73	0.59	0.83	1.03	0.15
MgO	–	–	0.92	–	–	–	–	–	0.54	–	–	–	–	–	0.55	–	–	–	–	–
CaO	0.11	0.05	4.66	2.56	0.07	0.21	0.08	0.99	2.88	1.00	0.37	0.24	0.38	0.19	3.03	0.95	1.74	0.16	0.28	0.74
Na_2O	11.18	0.81	1.04	1.98	11.10	10.61	0.78	3.88	2.22	3.86	4.19	3.77	4.60	11.27	1.73	3.25	3.06	10.86	1.53	4.25
K_2O	0.55	15.40	5.78	9.36	0.44	0.49	14.82	7.48	7.59	8.38	9.51	9.65	10.02	0.46	8.15	9.80	8.28	0.34	12.89	10.16
Total	92.62	99.35	80.79	88.91	90.30	86.39	99.39	78.81	81.89	82.53	84.46	88.28	91.52	94.34	83.31	91.57	82.55	90.19	102.20	99.68
Si	34.25	3.02	8.46	12.99	34.37	34.13	3.02	8.57	8.37	8.48	8.51	12.98	12.60	34.11	8.48	13.04	12.59	34.30	3.04	2.96
Al	13.83	0.92	3.47	4.99	13.67	13.78	0.92	3.43	3.57	3.51	3.43	5.02	5.41	13.94	3.44	4.93	5.43	13.62	0.95	1.03
Fe^{3+}	0.19	0.06	0.03	0.06	0.16	0.28	0.07	0.04	0.06	0.06	0.07	0.11	0.09	0.30	0.05	0.12	0.11	0.37	0.03	0.01
Mg	–	–	0.23	–	–	–	–	–	0.13	–	–	–	–	–	0.13	–	–	–	–	–
Ca	0.07	0.00	0.83	0.63	0.04	0.14	–	0.18	0.52	0.18	0.06	0.06	0.09	0.11	0.53	0.23	0.47	0.10	0.01	0.04
Na	12.41	0.07	0.34	0.89	12.63	12.66	0.07	1.31	0.72	1.25	1.33	1.70	2.02	12.28	0.55	1.41	1.48	12.38	0.13	0.37
K	0.40	0.92	1.23	2.75	0.33	0.38	0.88	1.66	1.62	1.78	1.99	2.87	2.89	0.33	1.71	2.80	2.64	0.26	0.73	0.59
E%	8.30	−1.70	−5.50	3.00	6.00	5.60	3.00	4.20	−0.30	5.30	1.70	9.40	8.00	10.90	−2.90	8.20	9.70	8.90	10.80	0.00
Si/Al	2.48	3.30	2.44	2.60	2.51	2.48	3.29	2.50	2.34	2.42	2.48	2.58	2.33	2.45	2.47	2.64	2.32	2.52	3.19	2.87

n: number of analyses; Cbz: chabazite; Ph: phillipsite; Anl: analcime; Kfs: authigenic K-feldspar; San: igneous sanidine
E% = balance error = $100(Al + Fe^{3+} - 2Mg - 2Ca - Na - K)/(2Mg + 2Ca + Na + K)$

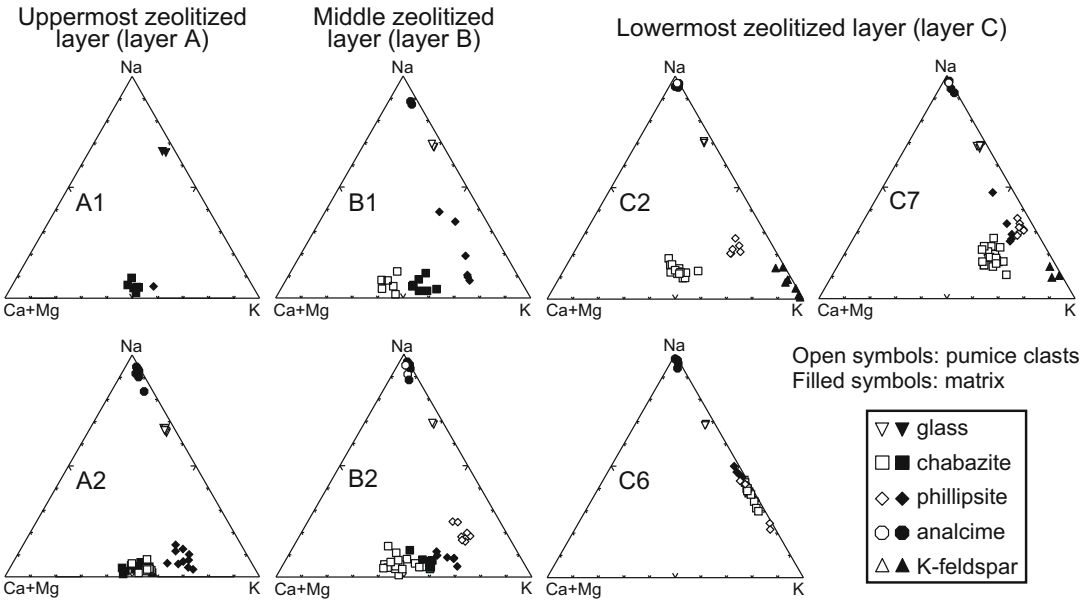

Figure 6. Triangular mole fraction diagram of exchangeable cations in zeolites and of mono- and divalent cations in K-feldspar and glasses from the Nettetal zeolite deposit.

and MgO and a strong depletion of Na_2O in most pumice clasts replaced by chabazite. Potassium exhibits only minor variation. The variability of the TiO_2 contents in fresh pumice clasts, however, allows no quantification of the possibly subtle changes of SiO_2 and Al_2O_3.

An estimation of the mass change of zeolitized matrix is complicated by sample preparation difficulties because it was impossible to treat cemented, zeolitized samples in the same manner as friable, fresh ash. Assuming immobility for TiO_2, however, this element can also be used as a 'contamination monitor', and fresh and zeolitized samples having the same TiO_2 contents can be compared. Based on this assumption, CaO and MgO were enriched and Na_2O and K_2O were slightly depleted in matrix samples of layers A and B (Table 3, Figure 5). Matrix samples of layer C showed no clear evidence for mass change, especially Na (Table 3, Figure 5). Matrix samples from which coarse contaminating particles (generally >2 mm) were manually removed, had the same Si/Al ratio as fresh ash having the same TiO_2 content. Matrix samples ground in bulk, however, had slightly higher Si/Al ratios, probably due to increased contamination with quartz clasts (Table 3, Figure 5).

EXPERIMENTAL SYNTHESIS RESULTS

The results of laboratory synthesis are presented in Figures 8–12. Chabazite, phillipsite, analcime, and K-feldspar were identified as newly-formed minerals under the investigated experimental conditions.

In all experiments, the reaction sequence of mineral formation was chabazite/phillipsite then phillipsite + analcime then analcime + K-feldspar, independent of temperature, solution composition, solid/liquid ratio, and grain-size (Figures 8–10). Chabazite and phillipsite were apparently metastable transition phases with respect to analcime and K-feldspar, at least at temperatures of 200 and 150ºC. At 100ºC, only chabazite with some phillipsite was observed in experiments with 0.01 M NaOH and 0.005 M NaOH + 0.005 M KOH solutions, up to 400 days.

Temperature, solution composition, solid/liquid ratio and grain-size, however, seemed to influence the alteration rate, as shown by the mineral contents of synthesis products. Increasing temperature and hydroxide concentration accelerated the transformation process of the glass to chabazite/phillipsite and finally K-feldspar (Figure 8).

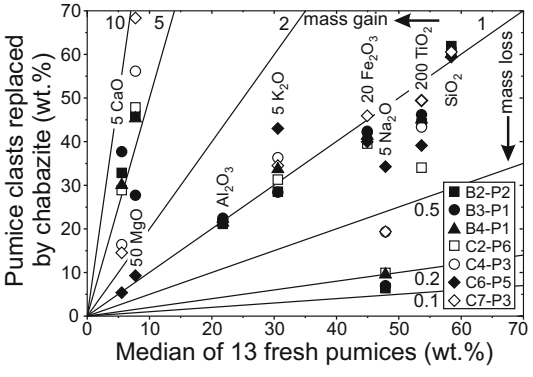

Figure 7. Isocon plot for pumice clasts replaced by chabazite of the Nettetal zeolite deposit.

https://doi.org/10.1346/000986002762090245 Published online by Cambridge University Press

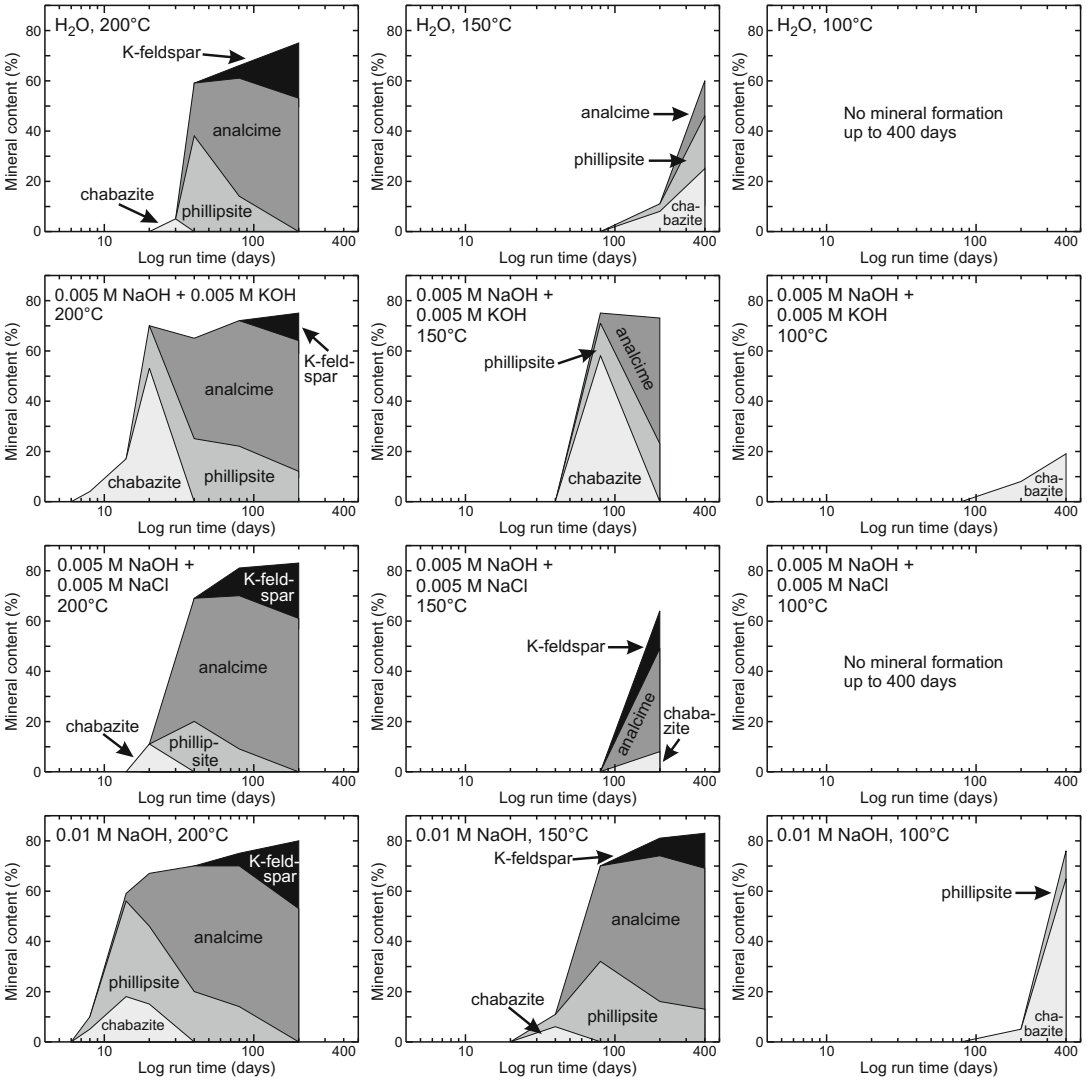

Figure 8. Results of experiments with ground pumice <63 μm and a constant solid/liquid ratio (0.5 g pumice, 25 mL solution).

A high solid/liquid ratio accelerated the formation of chabazite/phillipsite, but apparently retarded the formation of K-feldspar (Figure 9). Grain-size of 0.2−1.0 mm showed a slightly slower reaction rate than a starting material of <63 μm (Figure 9). The zeolitization of pumice fragments in experiments began at their exterior surfaces, and followed the same reaction sequence as for the ground material (Figure 10). Reaction progress, however, was slower than for the ground material of comparable weight. Fine-grained material was fully zeolitized after 20 days at 200ºC, whereas individual pumice fragments retained a fresh glassy core after 40 days and were totally zeolitized after 80 days. K-feldspar did not appear in pumice clasts, probably due to the reaction time being too short.

Chabazite formation was favored by low temperatures (100ºC), independent of solution composition. At higher temperatures (150 and 200ºC), an increase of the molar K/Na ratio of the bulk reacting system above that of the fresh glass (0.42) was necessary to increase the amount of chabazite (Figure 8). Bulk molar K/Na ratios were calculated by summing up the input of K and Na from both the solid starting material and the respective solution. This increase was achieved either by addition of K in the form of a KOH-bearing solution, resulting in a bulk molar K/Na of 0.50, or by removing some Na in the experiments simulating a slightly open system, causing a bulk molar K/Na of 0.49 (Figure 11a). Reaction of the glass with distilled water at 200ºC for 1 week resulted in a significant loss of Na, whereas the

https://doi.org/10.1346/000986002762090245 Published online by Cambridge University Press

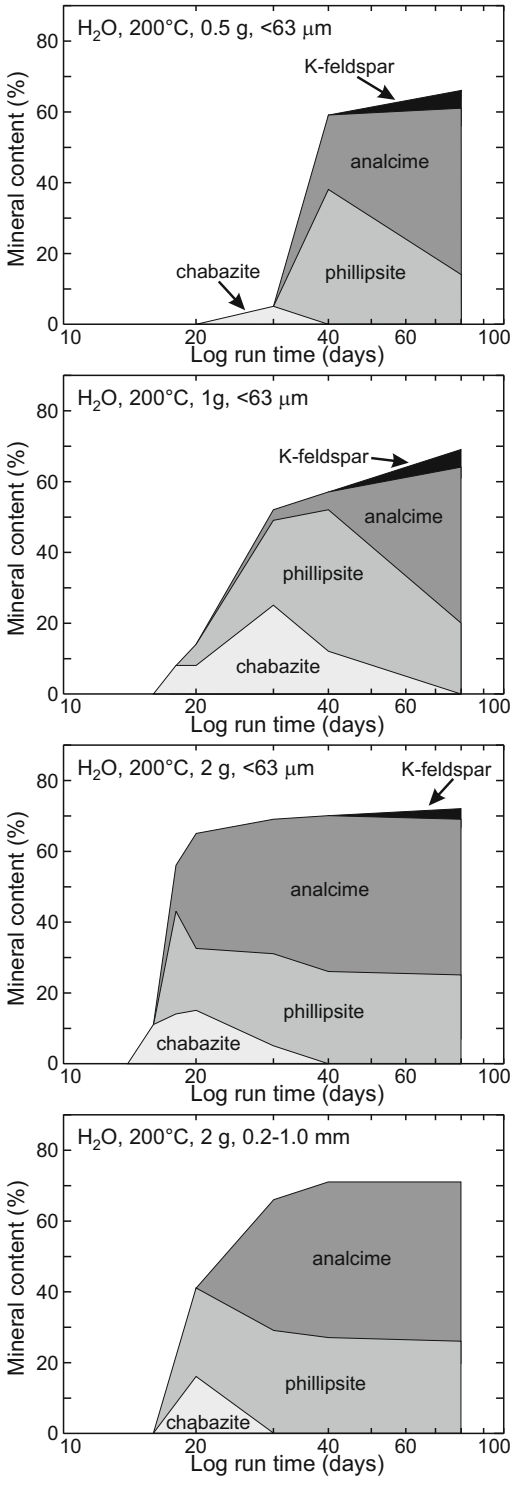

Figure 9. Results of experiments with distilled water (25 mL) at 200ºC and varying solid/liquid ratios and grain-size.

K content was nearly unaffected (Table 2, samples 'EX' and 'EX leach'). Chabazite did not form in the $Ca(OH)_2$ solution (Figure 11b).

Phillipsite formation was favored by temperatures $\geqslant$150ºC, increasing reaction time, and Na-dominated solution (Figure 8). Only small amounts of phillipsite formed in a slightly open system. In contrast to chabazite, large amounts of phillipsite formed in the $Ca(OH)_2$ solution (Figure 11).

Analcime formation was favored by temperatures >150ºC, the addition of Na, long reaction times, and high solid/liquid ratios (Figures 8 and 9).

The formation of K-feldspar at the expense of precursor zeolites was favored by high temperatures and long reaction times, possibly also by Cl^--containing solutions and low solid/liquid ratios (Figures 8 and 9). The triclinicity index of experimentally formed K-feldspars was ~0, because only a 131 reflection was observed (Goldsmith and Laves, 1954), and their structural state corresponds to high sanidine because of the 204 reflection at 50.79–50.87º2θ CuKα (Wright, 1968).

The Si/Al ratios of the synthetic zeolites ranged from 2.27 to 2.45 (median 2.34) for K-feldspar-free assemblages, independent of solid/liquid ratio, and the hydroxide concentration of reacting solution. Phillipsite and analcime in K-feldspar-bearing assemblages had slightly lower Si/Al ratios (median 2.29). Analcime and K-feldspar were of nearly Na- and K-end-member composition, respectively, whereas phillipsite and chabazite had variable atomic K/Na, scattering around 1. Chabazite was slightly richer in Ca and K, compared with accompanying phillipsite.

The cation-exchange experiments with chabazite using groundwater resulted in a nearly complete exchange of Na by Ca, but only a slight decrease of K (Figure 12), showing that Na was less preferred than K. This result corresponds with the selectivity series of chabazite Na << K < Ca, as described by Dyer and Zubair (1998).

DISCUSSION

Any genetic model for the Nettetal zeolite deposit must be able to explain reasonably the following observations: (1) the distribution of zeolite species, especially its high variability between different matrix samples in a single layer or in different layers and between matrix and pumice clasts of the same sample; (2) the formation of Ca,K-rich chabazite from Ca-poor precursor glass; and (3) the occurrence of zeolitization in three distinct layers, intercalated by fresh ash.

The most important factors controlling the zeolite species formed during the alteration of volcanic glass are: (1) composition of glass; (2) solution composition; (3) closed *vs.* open system; (4) solid/liquid ratio; (5) hydroxide concentration of solution; (6) temperature;

https://doi.org/10.1346/000986002762090245 Published online by Cambridge University Press

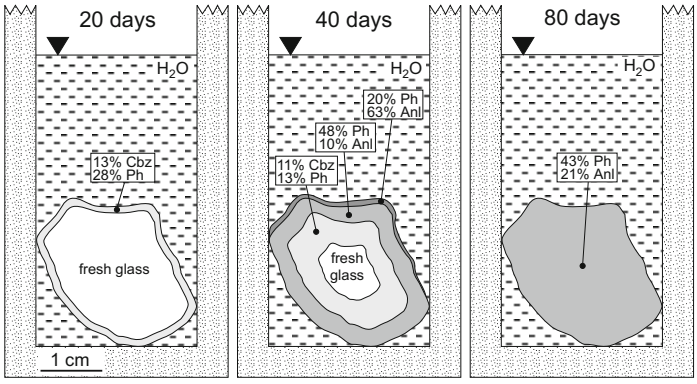

Figure 10. Set-up and results of experiments with individual pumice fragments (~2 g) and distilled water (25 mL) at 200ºC. Cbz = chabazite, Ph = phillipsite, Anl = analcime.

(7) grain-size distribution of glass; and (8) reaction time (see, *e.g.* Barth-Wirsching and Höller, 1989). These factors will be discussed with respect to the distribution of zeolite species, the formation of Ca,K-rich chabazite, and formation of three distinct zeolitized layers in the Nettetal zeolite deposit.

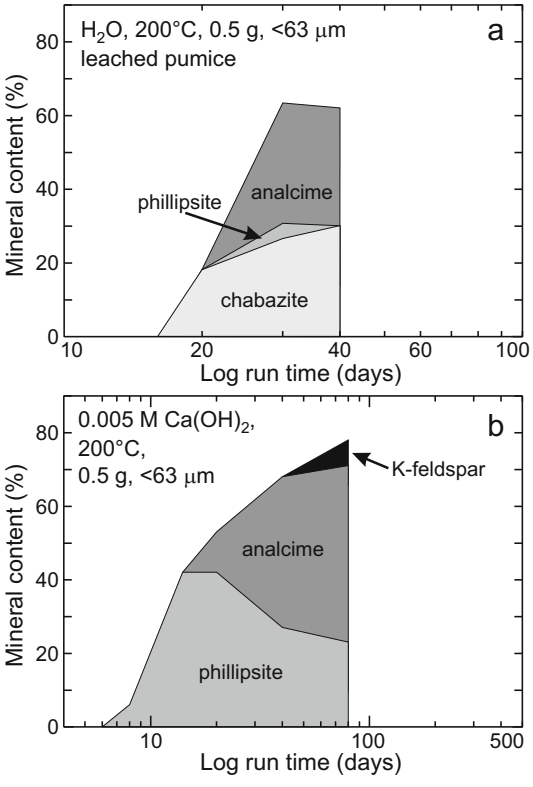

Figure 11. Results of experiments with ground pumice <63 μm (0.5 g) at 200ºC with (a) experimentally leached pumice and distilled water (25 mL) and (b) 0.005 M $Ca(OH)_2$ solution (25 mL).

Distribution of zeolite species

For the Nettetal zeolite deposit, the chemical variability of the precursor phonolitic glass materials is small; the Si/Al ratio and alkali content of bulk fresh pumice clasts, ash fractions <63 μm and glasses itself vary only slightly (Tables 1, 2 and 3, Figure 5). It does not seem possible that such slight variations should produce such different zeolite assemblages under otherwise constant alteration conditions.

Solution composition, especially at low concentrations, and temperature must be considered together in any discussion of which zeolite species formed at the beginning of alteration. Experimentally, the chabazite/phillipsite ratio depended strongly on temperature and solution composition. For example, at 100ºC, only

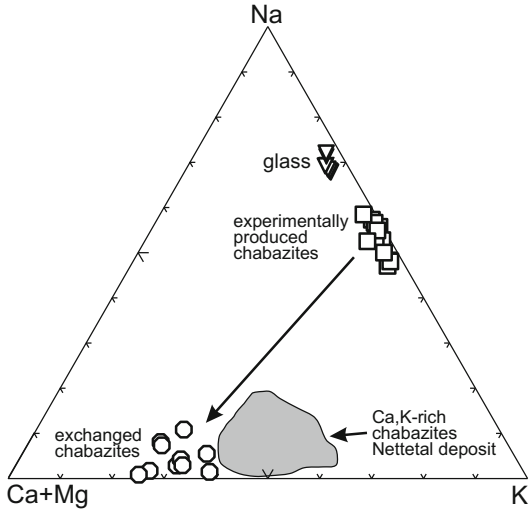

Figure 12. Triangular mole fraction diagram for exchangeable cations in experimentally produced, natural, and cation-exchanged chabazite (with Graz groundwater). Mono- and divalent cations in glasses from the Nettetal deposit are shown for comparison.

https://doi.org/10.1346/000986002762090245 Published online by Cambridge University Press

chabazite formed, independent of solution composition, *i.e.* at bulk molar K/Na ratios $\geqslant 0.31$. At $\geqslant 150$ºC, chabazite and phillipsite formed in nearly equal amounts at a bulk molar K/Na of 0.31 and 0.42. Large amounts of chabazite required higher bulk K/Na ratios of ~0.50, obtained by addition of K from the solution or by leaching of the glass in a slightly open system. Therefore, the large amounts of chabazite in pumice clasts and in the uppermost part of layer A of the Nettetal deposit are probably related to an increase of K/Na of the reacting system through an input of K or a leaching of Na, or to alteration at <150ºC.

Variations of the solution composition caused by reaction with the glass or by leaching processes in a slightly open system as well as different solid/liquid ratios influencing the alteration rate can explain the formation of various zeolite assemblages observed in different matrix samples of a single layer or of different layers.

Solution pH, which is a primary control of the Si/Al in zeolites during formation (Wilkin and Barnes, 2000), was of little importance in the Nettetal deposit according to the alteration in a low to moderately alkaline groundwater system. Zeolites in the Nettetal deposit have the same or slightly higher Si/Al ratios as the precursor glass. This locally elevated Si/Al ratio of the zeolites was probably caused by partial dissolution of epiclastic quartz, which is a minor constituent of the fresh and zeolitized ash. The natural assemblage K-feldspar + analcime (bulk Si/Al $\approx$ 2.45) also requires the addition of Si, if Al is not removed. The bulk sample chemistry does not suggest a significant influx of externally derived silica, but it is consistent with silica redistribution between dissolved quartz and neoformed zeolites and K-feldspar. In experiments with no addition of silica, both the K-feldspar and the analcime had lower Si/Al ratios than their natural counterparts.

Temperature itself had a great influence on the alteration rate. The experimental reaction sequence of zeolite formation was generally chabazite/phillipsite then phillipsite + analcime then analcime + K-feldspar, which corresponds closely with that observed in the deposit, shown by SEM investigations (Figure 3a,b,d). This sequence did not change with solution composition, hydroxide concentration, solid/liquid ratio, grain-size, or temperature, but the time necessary to run through this reaction sequence was strongly influenced by temperature. At 200ºC, chabazite and phillipsite were metastable transition phases, ultimately reacting to analcime + K-feldspar after 40 days. At 150ºC, the formation of K-feldspar was also influenced by solution composition. At 100ºC, neither analcime nor K-feldspar was observed in experiments $\leqslant$400 days. Dibble and Tiller (1981), however, showed that chabazite can be metastable with respect to analcime + K-feldspar even at temperatures <100ºC. The assemblage of chabazite + phillipsite still existing today in the zeolitized layers suggests low-temperature alteration of the Nettetal ash flow.

Grain-size significantly influenced the alteration rate, but the type and sequence of zeolite species formed did not change. Therefore, the different zeolitization of matrix and pumice clasts, *i.e.* the alteration of glass shards in the matrix to mainly analcime and the occurrence of fresh pumice in zeolitized matrix as well as the widespread preservation of chabazite in pumice clasts can be related to the different grain-size and reactivity of these two materials.

Reaction time influenced zeolite formation in such a way that zeolite species and zeolite assemblages changed with time at otherwise constant conditions. Therefore, various zeolite assemblages can be simply obtained by changing critical zeolite-forming conditions, *e.g.* by drying up of the reacting system or by quenching. From these experimental data, the various zeolite assemblages in the different zeolitized layers of the Nettetal deposit appear to be related to varying duration of alteration in different layers at otherwise constant conditions. The upper part of layer C represents the most advanced stage of alteration, whereas chabazite-rich pumice clasts and the matrix of the uppermost part of layer A represent very early stages of alteration.

Formation of Ca,K-rich chabazite

The high Ca content of chabazite (and phillipsite) in the Nettetal deposit can theoretically be explained in two ways. Chabazite could have become Ca rich by (1) a direct formation in a Ca-bearing solution or (2) a post-zeolitization cation exchange. Experimental alteration of the phonolitic glass with $Ca(OH)_2$ solution, however, showed that a Ca-rich reacting solution does not favor chabazite crystallization, at least at 200ºC. In contrast, Ca,K-rich chabazites were easily obtained in cation-exchange experiments of precursor Na,K-rich chabazite with solutions of low-Ca concentration. Furthermore, if chabazite was indeed a wide-spread precursor phase of analcime, the transformation of a Ca,K-rich chabazite to the Na-rich mineral analcime would have required a significant addition of Na. Therefore, the formation of Ca,K-rich chabazite by Ca-Na exchange of a previously-formed Na,K-rich chabazite seems to be more probable than a direct formation.

Formation of zeolites in three distinct layers

A variety of models has been proposed for the zeolitization of pyroclastic deposits in non-marine, non-saline, non-alkaline lake settings. One of the most widely proposed models is zeolitization by percolating groundwater in an open system (Hay and Sheppard, 1977), in which descending meteoric water becomes chemically modified by interaction with glass, leading to the crystallization of zeolites from solution in deeper parts of the pyroclastic deposit. This results in the more or less vertical mineralogical zonation of open-system zeolite deposits. A regular mineralogical zonation, however, was not observed in the Nettetal deposit;

zeolitization occurred in three distinct layers intercalated with totally fresh ash, suggesting that the classic open-system setting was unlikely.

Recently, a closed-system zeolitization process was proposed for the Yellow Neapolitan Tuff (de'Gennaro *et al.*, 2000). Zeolite formation was assumed to have been related to trapped water (10−25 wt.%) of phreatomagmatic origin and the preservation of elevated temperatures for a sufficiently long time to allow zeolitization. This led to a zeolitization predominantly in the center of cooling units, because high cooling rates at the top, bottom, and distal, thinner parts prevented extensive zeolite formation in these places. The Nettetal ash flow is composed of 14 flow units (Jandausch, 1980) but can be considered as one cooling unit due to deposition of the whole sequence within a few days or even hours (Schmincke *et al*., 1999). Emplacement temperature has been estimated to be in the range 300−600ºC (occurrence of charcoal, but no signs of welding, Meyer, 1988). Bogaard and Schmincke (1984), however, suggested that the flow was dry during initial deposition, which would contradict zeolitization by trapped phreatomagmatic water in a closed system.

In contradiction to the model of de'Gennaro *et al.* (2000), Hall (1998) pointed out that the removal of interstitial acid waters is a prerequisite for zeolitization of volcaniclastic deposits. Such interstitial waters would have had a pH of <1, which would have made zeolitization impossible. In his model, flushing with fresh water would have been necessary to remove acids, but this would have cooled the deposit and slowed down reaction kinetics to a degree that zeolitization was highly retarded. Therefore, Hall (1998) proposed that some kind of reheating was needed to zeolitize a volcaniclastic deposit within a reasonable time after it has been flushed with fresh water. The Laacher See volcanic eruption, however, was the last significant volcanic event in the studied area, and no significant reheating of the ash flow is obvious. In conclusion, none of these three existing models can account for all volcanological and mineralogical features observed in the Nettetal deposit.

Frechen (1971), Schmincke (1977) and Jandausch (1980) suggested earlier that at least a part of the zeolitization process was related to interaction of glass with groundwater. Judging from the experimental synthesis results, a promising place for such zeolitization would have been the stagnant fringe water zone above the groundwater table. This zone is a more or less closed system without significant water recharge (Ronen *et al.*, 1997). In such a milieu, solution compositions suitable for zeolite formation could have been attained rather quickly by water-glass interaction. This fringe water zone contrasts with deeper zones of the groundwater column, in which the system is efficiently recharged with fresh water and solution compositions suitable for zeolite formation could not build up. This results in a lack of zeolitization in the deepest part of the ash flow, despite the fact that it had been in contact with groundwater nearly since the emplacement of the flow.

CONCLUSIONS

All arguments resulting from field and experimental data suggest that zeolitization of phonolitic glass in the Nettetal deposit is the result of alteration by groundwater, probably in the fringe water zone. The different zeolitized layers could represent different paleo-groundwater tables. The accumulation of pyroclastic material during the Laach volcanic eruption in receiving river beds possibly led to a significant temporary rise of the groundwater level. This was followed by a rather quick erosion of the soft material, resulting in a possibly stepwise decrease of groundwater level. Assuming otherwise constant alteration conditions, the different stages of matrix zeolitization could indicate that the groundwater table remained at different levels for varying times. The influx of groundwater into the possibly still hot pyroclastic deposit would have resulted in a significant temperature decrease, at least below the boiling point of ~160ºC at 5 bar for the deepest parts and of ~125ºC at 2 bar for the upper parts, because fumarolic activity associated with the Nettetal ash flow has not been observed. This influx could also have diluted the small amount of eruption-related, acid water, if any was present. A thorough flushing seems not to have been necessary, because volcanic glass is able to neutralize acid pore solutions by proton acceptance and release of alkali and alkaline-earth cations (de'Gennaro *et al.*, 2000).

The following sequence of events causing zeolitization in the Nettetal deposit seems to be most probable.

(1) Deposition of a hot (300−600ºC), dry, phonolitic ash flow within a few days.

(2) Rise of groundwater table up to layer A and cooling of the flow to $\leqslant$125ºC, if it was still hotter before the groundwater entered the flow.

(3) Zeolitization of layer A, resulting in the formation of chabazite, phillipsite and analcime in the matrix, whereas the pumice clasts remained unaltered.

(4) Fall of groundwater level just below layer B, with subsequent zeolitization of layer B, resulting in the formation of chabazite, phillipsite and predominantly analcime in the matrix and the alteration of pumice clasts to mainly chabazite at the bottom of the layer.

(5) Fall of groundwater level to the bottom of layer C, with subsequent zeolitization of the matrix to phillipsite and mainly analcime and a nearly complete alteration of pumice clasts to mainly chabazite.

(6) Possibly irregular rise of groundwater level to the top of layer C, with associated zeolitization to varying degrees. Long-term stability of groundwater level near the top of layer C (until now), resulting in a highly advanced alteration of the matrix to analcime and K-feldspar and the complete zeolitization of the pumice clasts to mainly chabazite.

ACKNOWLEDGMENTS

Our thanks are due to F. Mumpton for helpful suggestions and revising the manuscript. G. Hoinkes is thanked for providing access to the SEM at the Institut für Mineralogie und Petrologie, Karl-Franzens-Universität Graz. Thorough reviews by D.W. Ming, R.L. Hay, and D.C. Bain are gratefully acknowledged. This work was supported financially by the FWF-project P11517-GEO.

REFERENCES

Adabbo, M., Langella, A., de'Gennaro, M. and Guerriero, A. (1994) Sedimentary zeolites from East Eifel volcanic district (Germany). *Materials Engineering,* **5,** 107–118.

Barth-Wirsching, U. and Höller, H. (1989) Experimental studies on zeolite formation conditions. *European Journal of Mineralogy,* **1,** 489–506.

Bogaard, P.V.D. and Schmincke, H.-U. (1984) The Eruptive Center of the Late Quaternary Laacher See Tephra. *Geologische Rundschau,* **73,** Heft 3, 933–980.

Bogaard, P.V.D. and Schmincke, H.-U. (1995) $^{40}Ar/^{39}Ar$ ages of sanidine phenocrysts from Laacher See Tephra (12,900 years BP): chronostratigraphic and petrological significance. *Earth and Planetary Science Letters,* **133,** 163–174.

de'Gennaro, M., Cappelletti, P., Langella, A., Perrotta, A. and Scarpati, C. (2000) Genesis of zeolites in the Neapolitan Yellow Tuff: geological, volcanological and mineralogical evidence. *Contributions to Mineralogy and Petrology,* **139,** 17–35.

Dibble, W.E. and Tiller, W.A. (1981) Kinetic model of zeolite paragenesis in tuffaceous sediments. *Clays and Clay Minerals,* **29,** 323–330.

Dyer, A. and Zubair, M. (1998) Ion-exchange in chabazite. *Microporous and Mesoporous Materials,* **22,** 135–150.

Frechen, J. (1971) Siebengebirge am Rhein, Laacher Vulkangebiet, Maargebiet der Westeifel. *Sammlung Geologischer Führer,* **56,** Gebrüder Bornträger, Berlin, Stuttgart.

Goldsmith, J.R. and Laves, F. (1954) The microcline-sanidine stability relations. *Geochimica et Cosmochimica Acta,* **5,** 1–19.

Govindaraju, K. (1994) 1994 Compilation of working values and description for 383 geostandards. *Geostandards Newsletter,* **18,** 1–158.

Grant, J.A. (1986) The Isocon-Diagram – A simple solution for Gresens' equation of Metasomatic alteration. *Economic Geology,* **21,** 751–754.

Hall, A. (1998) Zeolitization of volcaniclastic sediments: the role of temperature and pH. *Journal of Sedimentary Research,* **68,** 739–745.

Harms, E. and Schmincke H.-U. (2000) Volatile composition of the phonolitic Laacher See magma (12,900 yr BP): implications for syn-eruptive degassing of S, F, Cl and H_2O. *Contributions to Mineralogy and Petrology,* **138,** 84–98.

Hay, R.L. (1977) Geology of zeolites in sedimentary rocks. Pp. 53–64 in: *Mineralogy and Geology of Natural Zeolites* (F.A. Mumpton, editor). Reviews in Mineralogy, **4**. Mineralogical Society of America, Washington, D.C.

Hay, R.L. and Sheppard, R.A. (1977) Zeolites in open hydrologic systems. Pp. 93–102 in: *Mineralogy and Geology of Natural Zeolites* (F.A. Mumpton, editor). Reviews in Mineralogy, **4**. Mineralogical Society of America, Washington, D.C.

Höller, H. and Wirsching, U. (1974) Experimente zur Zeolithbildung durch hydrothermale Umwandlung. Zur Entstehung von Chabasit, Phillipsit und Analcim aus den glasigen Bestandteilen der Bims-Staubtuffe des Laacher Vulkangebietes. *Contributions to Mineralogy and Petrology,* **46,** 49–60.

Jandausch, P. (1980) Aufbau und Entstehung des Traß-Profils in der Grube Meurin/Eifel. Unveröffentlichte Diplomarbeit, Universität Bochum, Germany, 102 pp.

Lister, B. (1982) Evaluation of Analytical Data: A Practical Guide to Geoanalysis. *Geostandards Newsletter,* **6,** 175–205.

Meyer, W. (1988) *Geologie der Eifel.* E. Schweizerbart'sche Verlagsbuchhandlung, Stuttgart, Germany, 615 pp.

Rock, N.M.S., Webb, J.A., McNaughton, N.J. and Bell, G.D. (1987) Nonparametric estimation of averages and errors for small data-sets in isotope geosciences: a proposal. *Chemical Geology,* **66,** 163–177.

Ronen, D., Scher, H. and Blunt, M. (1997) On the structure and flow processes in the capillary fringe of phreatic aquifers. *Transport in Porous Media*, **28,** 159–180.

Schmincke, H.-U. (1977) Eifel-Vulkanismus östlich des Gebietes Rieden-Mayen. *Fortschritte der Mineralogie, Beiheft 2,* **55,** 1–31.

Schmincke, H.-U., Park, C. and Harms, E. (1999) Evolution and environmental impacts of the eruption of Laacher See Volcano (Germany) 12,900 a BP. *Quaternary International,* **61,** 61–72.

Wilkin, R.T. and Barnes, H.L. (2000) Nucleation and growth kinetics of analcime from precursor Na-clinoptilolite. *American Mineralogist,* **85,** 1329–1341.

Wright, T.L. (1968) X-ray and optical study of alkali feldspar: II. An X-ray method for determining the composition and structural state from measurement of 2θ values for three reflections. *American Mineralogist,* **53,** 88–104.

(*Received 9 October 2001; revised 4 July 2002; Ms. 592*)